









Analytical and computational study of three coptic icons in Saint Mercurius Monastery, Egypt

Ahmed Refaat ¹, Diaa Atta ¹, Osama Osman ¹, Abdel Aziz Mahmoud ¹, Sherif El-Kohadary ²,
Wadeea Malek ³, Marco Ferretti ⁴, Hanan Elhaes ⁵, Medhat Ibrahim ^{1,*}

¹Spectroscopy Department, National Research Center, 33 El-Bohouth Str., 12622 Dokki, Giza, Egypt

²Building Physics and Environment Institute, Housing & Building National Research Center (HBRC), 12311 Dokki, Giza, Egypt

³Scientific Group for Coptic Icons, Ministry of Antiquities, Cairo, Egypt

⁴Consiglio Nazionale delle Ricerche, Istituto di Scienze del Patrimonio Culturale, A.d.R. RM1, Via Salaria km 29.300, 00015 Montelibretti (Rome), Italy

⁵Physics Department, Faculty of Women for Arts, Science and Education, Ain Shams University, 11757, Cairo, Egypt

*corresponding author e-mail address: medahmed6@yahoo.com | Scopus ID [8641587100](https://orcid.org/0000-0001-8641-5871)

ABSTRACT

Three wooden Coptic icons located at Saint Mercurius Monastery in Tamooh, Giza, Egypt were comprehensively investigated in order to determine the possible causes of their deterioration. Samples from every paint used in each icon were collected spanning from the outermost varnish layer down to the ground layer. Investigation was carried out using Fourier-transform infrared spectroscopy (FTIR), scanning electron microscopy with energy dispersive spectroscopy (SEM-EDS), Energy-dispersive X-ray spectroscopy (EDX) and X-ray fluorescence (XRF). For interaction between the icon layers DFT calculations at B3LYP/6-31g(d,p) level were conducted in order to study the effect of humidity on the reactivity of the binder material and its possible role in the deterioration of the icons.

Keywords: *Coptic icons, FTIR, SEM-EDS, XRF and B3LYP/6-31g(d,p).*

1. INTRODUCTION

Coptic art refers to the art of Egypt produced by Egyptian Christians in late Roman, early Byzantine, early Arab and late Middle Ages. Icon is the word that describes a Coptic religious picture and is primarily associated with the paintings of the Orthodox Churches [1]. An icon is composed of five layers, support, usually a wooden panel, ground, binder, paint and varnish layer [2].

Although thousands of icons are found in churches and monasteries of Egypt, very limited information was available about them for a long time. Recently, studying Coptic icons has been an element of interest from different aspects including description, characterization and identification, dating, interpretation, conservation and restoration [1-5]. Like other historic structures, Coptic icons are deteriorating with aging especially when left without conservation and restoration. However, before trying to proceed with conservation and/or restoration of an icon, it is important to determine the possible sources and causes of deterioration [6].

The causes of deterioration of historic structures including Coptic icons can be biological, chemical and/or physical [6-10]. Spectroscopic and elemental analysis techniques have been extensively employed to study the causes of deterioration and effect of aging of different history and ancient structures in Egypt. The deteriorating black and red pastes used in decorating the wall of Qijmas El-Eshaqi Mosque in Cairo, Egypt were characterized and identified for the conservation process [11]. The dyes and organic stains used in silk textiles in Islamic Art museum in Cairo, Egypt were characterized as new approach for conservation treatment [12]. FTIR elucidated the changes in the chemical stability of archaeological bones as an effect of the burial

environment on crocodile bones from Hawara excavation in Fayoum, Egypt [13].

Molecular modeling approaches have also been recently applied to study cultural heritage materials [14]. Density functional theory (DFT) and wave function theory methods were employed to study the proto-isomerization mechanisms of indigo pigment and its derivatives [15]. Quantum mechanical calculations were used to study the molecular interaction between tannin dyes and protein-based historical textiles in order to identify the relative geometries and possible coordination modes [16]. Different time-dependent DFT methods were used to study the electronic structures of indigo in aqueous solution in correlation with UV-Visible spectroscopy [17]. DFT quantum mechanical calculations were also implemented to study the interaction of carbonate stones with oxalates and oxamates [18].

Nowadays molecular modeling is a promising tool to elucidate the structure as well as chemical and physical parameters of many systems whereas experimental tools are limited and/or expensive [19-21].

The three Coptic icons under investigation are for Saint Abaskhiroun, Saint George, and Saints Maximus and Domatius. This work is conducted in order to investigate the possible reasons for deterioration of the three icons using FTIR to study the molecular structure of the icons, SEM-EDS and XRF to study the chemical elemental composition of the icons and their surface morphology. Molecular modeling calculations are also used to theoretically investigate the interaction between the metal oxides, supposedly present in the icons, and the binder material, and effect of this interaction on the reactivity of the icons to the surrounding environment.

2. MATERIALS AND METHODS

2.1. Samples and Sample preparation.

Nine samples were collected from Saint Abaskhiroun Icon, seven samples were collected from Saint George Icon and eight samples were collected from Saints Maximus and Domatius icon. Samples were taken from the edges of the icons and/or from damaged areas using a scalpel. The collected samples were embedded in a transparent epoxy resin. The paint colors are as illustrated in table 1.

2.2. Instrumentation.

2.2.1. SEM-EDS.

SEM-EDS measurements were carried out by Philips (Inspect S, FEI Company, Holland) Scanning Electron Microscope (SEM) operated at 30 kV.

2.2.2. XRF.

Non-destructive X-ray Fluorescence analyses were performed by means of portable equipment in the CNR, Istituto per le Tecnologie Applicate ai Beni Culturali, Montelibretti, Rome, Italy.

2.2.3. Fourier-Transform Infrared Spectroscopy (FTIR).

Mid Infrared spectra are recorded using a portable ALPHA spectrometer (Bruker Optics, Germany) equipped with a ZnSe ATR crystal system. The spectra were acquired with 32 scans in the wavenumber range of 4000-400 cm^{-1} at room temperature and with 4 cm^{-1} spectral resolution.

2.3. Computational details.

Molecular modelling simulations were carried out to investigate the possible reasons for the fragility of painting layers in Coptic icons. In particular, we simulated the interactions between the metal oxides, such as Al_2O_3 , Fe_2O_3 and ZnO , supposedly contained in the pigments, and aspartic amino acid, supposedly contained in the binder (egg yolk), in adsorbed and complex states, with and without hydration. The model, built according to previous studies, was calculated with the GAUSSIAN09 program [22], installed on a workstation at the Spectroscopy Department, National Research Centre of Egypt, and optimized by the Density Functional Theory method B3LYP/6-31g (d,P). [23-25].

Table 1. Designation of the samples obtained from the three icons

Saint Abaskhiroun Icon		Saint George Icon		Saints Maximus and Domatius Icon	
Sample	Colour	Sample	Colour	Sample	Colour
1	Green	1	Green	1	Green
2	Grey	2	Yellow	2	Blue
3	Red	3	Red	3	Green with varnish
4	Blue	4	White	4	Blue with varnish
5	Red	5	Golden	5	Frame without varnish
6	White	6	Blue	6	Varnish from the face
7	Brown	7	Golden	7	Golden background
8	Green			8	Varnish over gold
9	Golden				

3. RESULTS

3.1. SEM-EDS.

The SEM micrographs of the samples obtained from Saint Abaskhiroun Icon, Saint George Icon, and Saints Maximus and Domatius Icon are shown in Fig. 1, 2 and 3 respectively. All samples showed coarse surfaces with the presence of microcracks reflecting the effect of humidity and suggesting the cement-like nature of the ground material which was confirmed by EDS, XRF and FTIR to be composed of gypsum and lead white. The presence of Na, K and Cl in the great majority of the samples reflects the

effect of environmental salinity on the icons which was found to be present on the outer layer of the icons, not reaching the ground layer.

The elemental compositions in terms of atomic percentage of samples from Saint Abaskhiroun icon, Saint George icon and Saints Maximus and Domatius icon are shown in Tables 2, 3 and 4 respectively. EDS results reflected the presence of C, O and Ca in all samples. Additionally, Mg, Al, Si, Cl, and K were found in all samples from Saint Abaskhiroun and Saint George icons.

Table 2. EDS elemental composition in atomic percentage of sample 1 to 9 from Saint Abaskhiroun Icon.

Element	Sample 1	Sample 2	Sample 3	Sample 4	Sample 5	Sample 6	Sample 7	Sample 8	Sample 9
C	61.24	84.91	65.40	57.58	49.27	78.72	58.49	72.48	50.01
N	1.92	-	-	-	-	-	-	-	-
O	32.62	13.86	30.07	36.51	40.67	19.91	36.52	25.69	38.85
Na	0.66	0.25	0.43	-	0.84	0.29	0.64	0.42	0.74
Mg	0.29	0.07	0.34	0.39	0.65	0.11	0.36	0.15	0.50
Al	0.51	0.17	0.37	0.67	1.16	0.18	0.62	0.22	3.13
Si	0.96	0.29	0.75	1.27	2.40	0.33	1.13	0.38	4.73

Analytical and computational study of three coptic icons in Saint Mercurius Monastery, Egypt

Element	Sample 1	Sample 2	Sample 3	Sample 4	Sample 5	Sample 6	Sample 7	Sample 8	Sample 9
P	0.06	0.02	0.15	0.49	0.38	0.02	0.09	0.02	-
S	0.47	-	-	0.56	0.95	-	0.60	0.16	-
Cl	0.23	0.15	0.63	0.60	0.50	0.06	0.25	0.10	0.22
K	0.07	0.04	0.05	0.23	0.20	0.05	0.09	0.05	0.26
Ca	0.84	0.19	1.10	1.26	2.57	0.25	1.10	0.29	0.73
Ba	0.04	-	-	0.02	-	-	-	-	-
Fe	0.08	-	0.09	0.14	0.29	0.04	0.11	0.05	0.43
Zn	0.02	-	-	0.28	0.10	-	-	-	-
Pb	-	0.05	0.61	-	-	0.03	-	-	-
Ti	-	-	-	-	-	-	-	-	0.05
Au	-	-	-	-	-	-	-	-	0.34

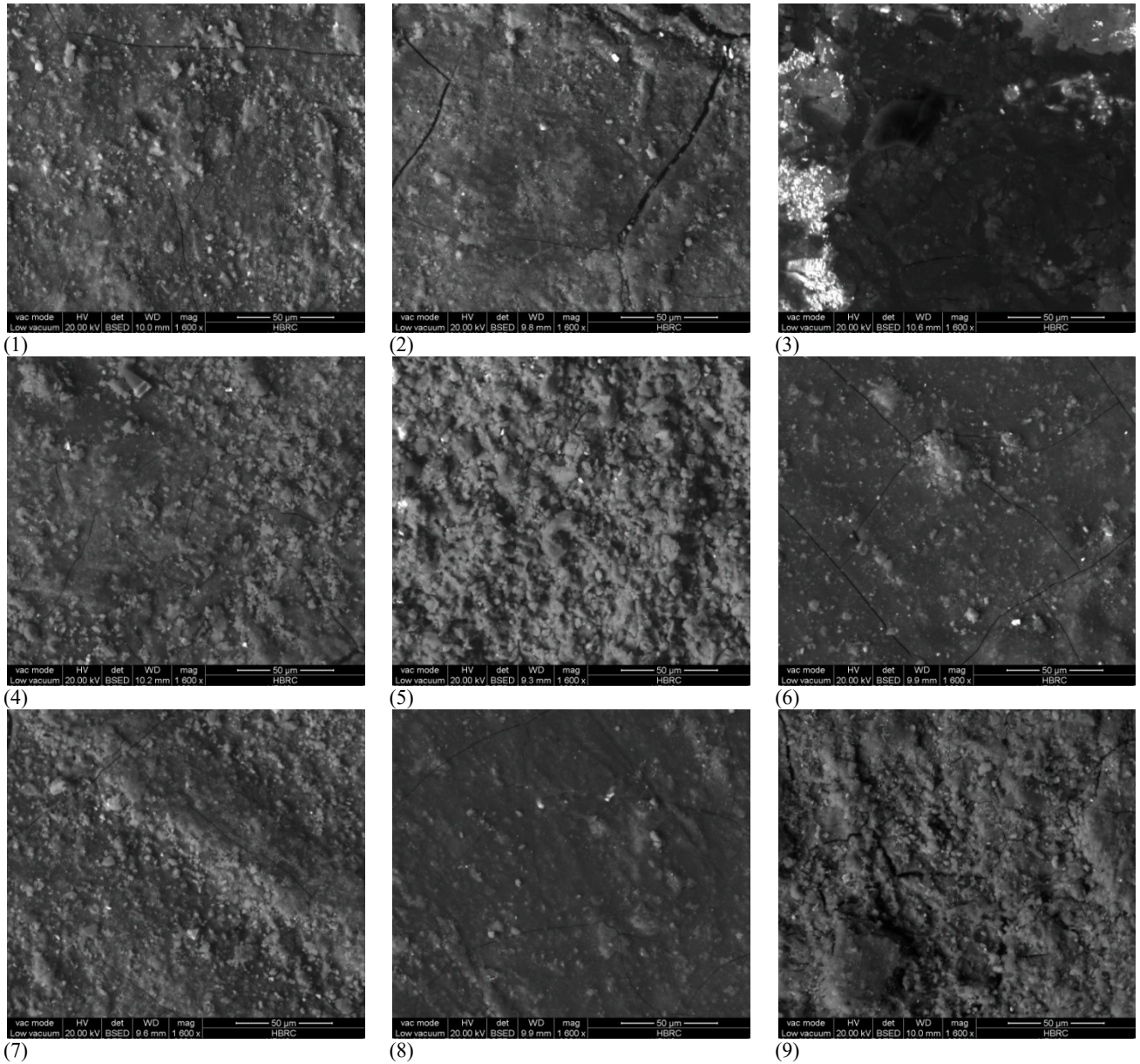
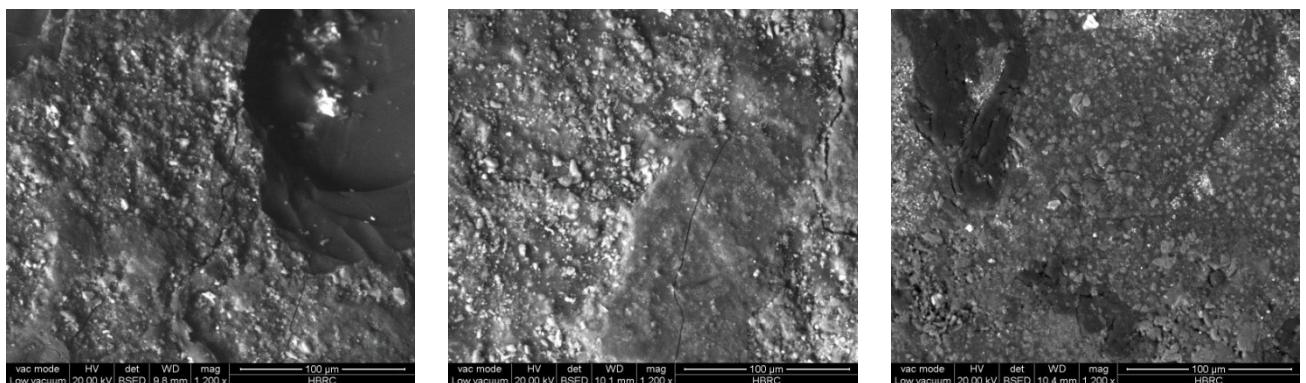


Figure 1. SEM Micrographs of samples 1 to 9 from Saint Abaskhiroun Icon.



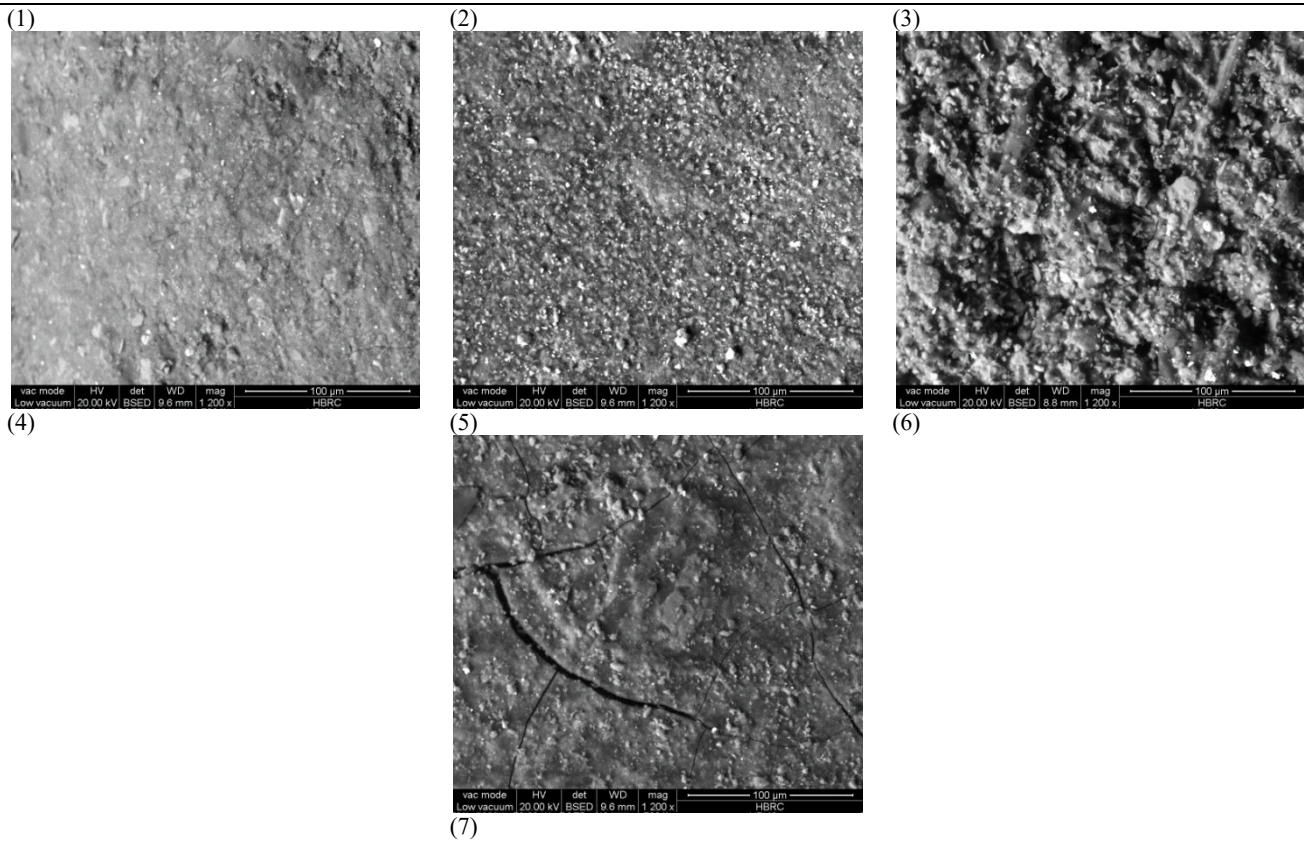
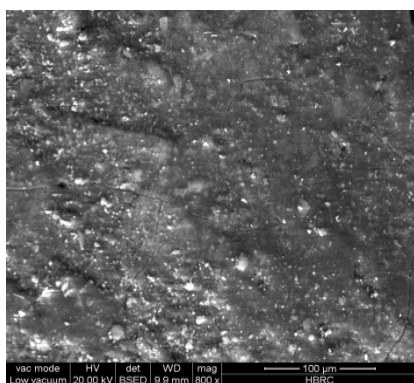


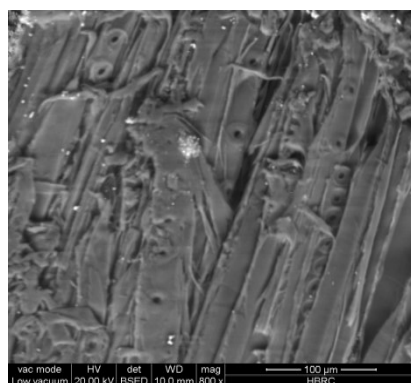
Figure 2. SEM Micrographs of samples 1 to 7 from Saint George Icon.

Table 3. EDS elemental composition in atomic percentage of samples 1 to 7 from Saint George Icon.

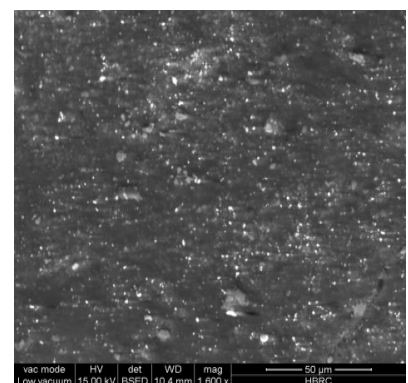
Element	Sample 1	Sample 2	Sample 3	Sample 4	Sample 5	Sample 6	Sample 7
C	74.83	64.28	67.62	55.03	55.95	56.50	61.96
N	--	--	--	--	--	4.18	--
O	23.40	31.44	28.25	37.73	37.64	32.79	33.88
Na	0.47	0.33	--	0.60	0.73	0.42	--
Mg	0.10	0.84	0.19	0.55	0.27	0.47	0.29
Al	0.18	0.58	0.64	1.09	0.50	1.07	0.64
Si	0.32	1.14	1.08	2.23	0.84	2.41	1.16
P	0.04	0.06	0.08	--	--	0.05	0.05
S	0.16	0.34	0.60	0.55	0.76	0.36	0.35
Cl	0.08	0.08	0.31	0.29	0.20	0.11	0.49
K	0.03	0.09	0.08	0.15	0.09	0.16	0.10
Ca	0.28	0.69	0.56	1.52	2.69	1.16	0.72
Ba	0.03	--	--	0.03	0.15	0.03	--
Fe	0.04	0.13	0.07	0.23	0.08	0.28	0.12
Zn	0.04	--	0.53	--	0.09	--	0.22
Co	--	--	--	--	--	0.02	--



(1)



(2)



(3)

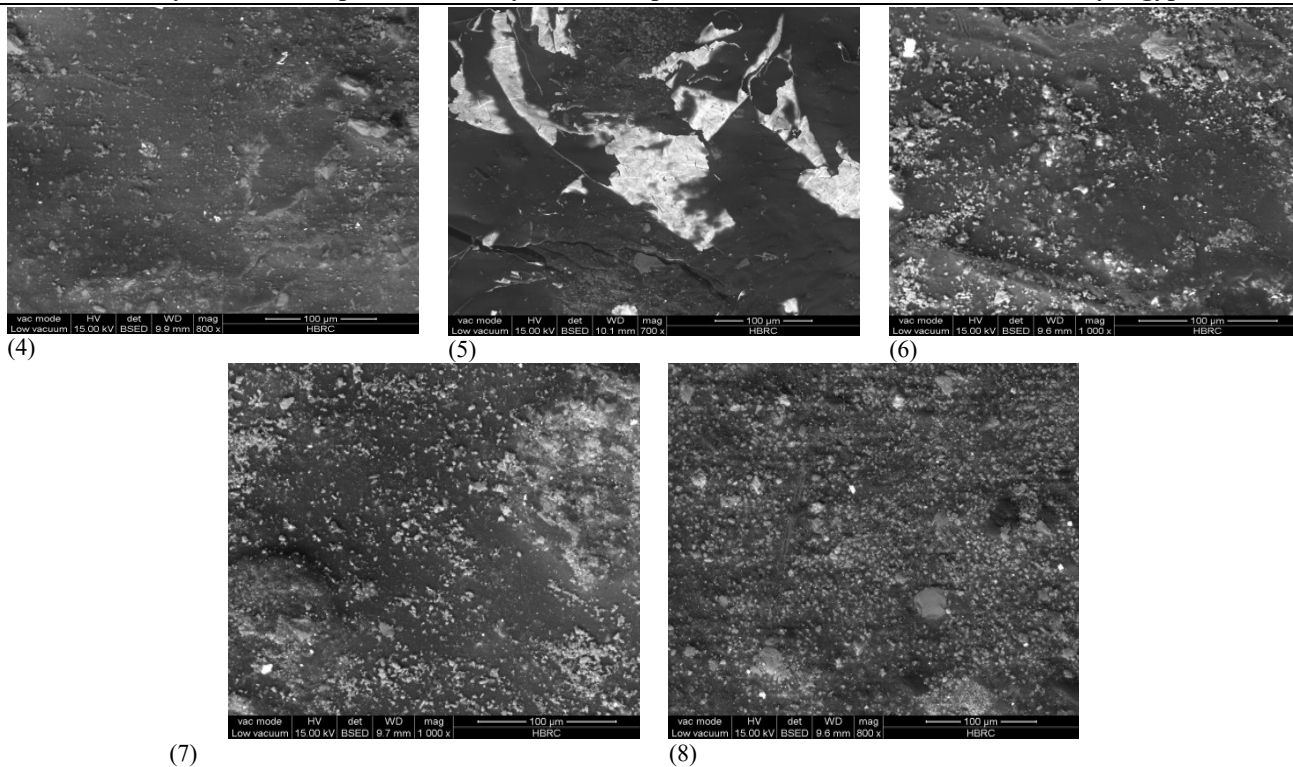


Figure 3. SEM micrographs of samples 1 to 8 from Saints Maximus and Domatius Icon.

Table 4. EDS elemental composition in atomic percentage of samples 1 to 8 from Saints Maximus and Domatius Icon.

Element	Sample 1	Sample 2	Sample 3	Sample 4	Sample 5	Sample 6	Sample 7	Sample 8
C	63.72	49.28	74.74	68.64	73.34	72.34	70.65	64.82
N	--	--	--	--	--	--	--	--
O	31.06	40.4	24.24	28.25	20.8	25.68	26.89	27.37
Na	0.81	1.34	0.6	0.6	--	0.24	0.27	2.33
Mg	0.27	0.17	--	0.23	--	0.46	0.17	0.15
Al	0.57	0.23	--	0.38	--	0.16	0.19	1.42
Si	1.13	0.35	--	0.69	--	0.31	0.27	1.92
P	--	--	--	0.07	--	--	0.05	0.11
S	0.61	0.3	--	0.29	--	0.11	0.23	0.84
Cl	0.21	0.19	--	0.1	--	0.05	0.12	0.17
K	0.14	--	--	0.07	--	--	--	0.17
Ca	1.32	7.75	0.19	0.69	0.27	0.63	1	0.46
Ba	--	--	--	0.69	--	--	--	--
Fe	0.19	--	--	--	--	--	0.16	0.24
Zn	--	--	--	--	--	--	--	--
Pb	--	--	0.23	--	--	--	--	--
Ti	--	--	--	--	--	--	--	--
Au	--	--	--	--	5.58	--	--	--

3.2 XRF.

It is well known that XRF has a higher penetrating power than EDS with a high spatial resolution, and is thus very useful for elemental analysis inside the sample [26].

XRF results indicated the presence of Si, Ca, Rb, Sr, Ba, Ti, Al in the ground layer and were detected in all samples, except for Sr, which was not found in the ground layer of Saint Maximus and Domatius icon. Fe was also present in all samples both in the ground and paint layers, probably in the form of Fe oxide. Pb and

Zn were present in all samples both in the ground and the paint layers, probably in the form of mixtures between lead white and zinc white. Six samples from Saints Maximus and Domatius icon, where the visible colour is neither green nor blue, showed traces of Cu. The obtained XRF profiles of samples from Saint Abaskhiroun icon, Saint George icon, and Saints Maximus and Domatius icon are illustrated in Tables 5, 6 and 7 respectively, displaying the elements most relevant to each colour.

Table 5. XRF profile of samples 1 to 9 from Saint Abaskhiroun Icon

Sample	Assignment
1	<ul style="list-style-type: none"> Traces of Co, probably cobalt blue. As and traces of Sb in a lower layer, probably from previous repainting trial.
2	<ul style="list-style-type: none"> Pb (also detected by EDS) probably representing lead white.
3	<ul style="list-style-type: none"> Hg, probably cinnabar.

Sample	Assignment
	<ul style="list-style-type: none"> • Fe (also detected by EDS) probably ochre or earth colour. • Pb (also detected by EDS) probably representing lead white.
4	<ul style="list-style-type: none"> • Fe (also detected by EDS) and traces of Co, probably reflecting a mixture of Prussian blue and cobalt blue. • Zn (also detected by EDS).
5	<ul style="list-style-type: none"> • Fe (also detected by EDS) and traces of Hg, probably representing a mixture of red ochre and cinnabar.
6	<ul style="list-style-type: none"> • Fe (also detected by EDS) probably ochre or earth colour. • Pb (also detected by EDS) probably representing lead white.
7	<ul style="list-style-type: none"> • Fe (also detected by EDS) probably ochre or earth colour.
8	<ul style="list-style-type: none"> • Fe (also detected by EDS) probably ochre or earth colour. • Traces of As, probably orpiment. • Au and Ag, gilding in a lower layer.
9	<ul style="list-style-type: none"> • Fe (also detected by EDS) probably ochre or earth colour. • Au and Ag, gilding in a lower layer. • Ti.

Table 6. XRF profile of samples 1 to 7 from Saint George Icon

Sample	Assignment
1	<ul style="list-style-type: none"> • As, probably orpiment.
2	<ul style="list-style-type: none"> • Fe (also detected by EDS) probably ochre or earth colour. • Au and Ag, gilding in a lower layer.
3	<ul style="list-style-type: none"> • Traces of As, probably orpiment. • Fe probably ochre or earth colour, and Pb that may be attributed to lead white from the ground layer or red lead (Pb₃O₄).
4	<ul style="list-style-type: none"> • Pb, lead white.
5	<ul style="list-style-type: none"> • As, probably orpiment.
6	<ul style="list-style-type: none"> • Co (also detected by EDS), probably reflecting cobalt blue.
7	<ul style="list-style-type: none"> • Traces of Au and Ag, gilding layer. • Fe (also detected by EDS), probably ochre or earth colour.

Table 7. XRF profile of samples 1 to 9 from Saints Maximus and Domatius Icon

Sample	Assignment
1	<ul style="list-style-type: none"> • Au and Ag, probably gilding in a lower layer. • Fe (also detected by EDS), probably ochre or earth colour in the paint layer. • Traces of Cu.
2	<ul style="list-style-type: none"> • Traces of Co and Cu, probably green-blue pigment.
3	<ul style="list-style-type: none"> • Pb (also detected by EDS), probably lead white. • Traces of Cu.
4	<ul style="list-style-type: none"> • Fe, probably ochre or earth colour in the paint layer. • Au and Ag, gilding in a lower layer. • Cu.
5	<ul style="list-style-type: none"> • Traces of Au and Ag, probably gilding in a lower layer.
6	<ul style="list-style-type: none"> • Cu, probably related to a green Cu-based pigment. • As, probably representing orpiment as part of the yellow paint.
7	<ul style="list-style-type: none"> • Fe (also detected by EDX) probably ochre or earth colour.
8	<ul style="list-style-type: none"> • Fe (also detected by EDX) probably ochre or earth colour.

3.3. FTIR.

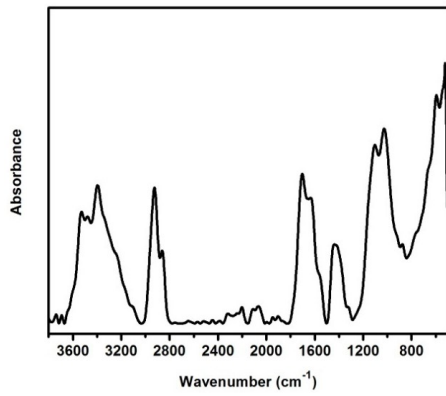
FTIR analysis was conducted in order to confirm the results obtained by EDS and XRF, particularly concerning the presence of a proteinaceous material, mostly egg yolk, in the binder layer as well as the presence of metal species, mostly metal oxides that are essentially present in paint materials.

FTIR absorbance spectra of samples from Saint Abaskhiroun icon, Saint George icon, and Saints Maximus and

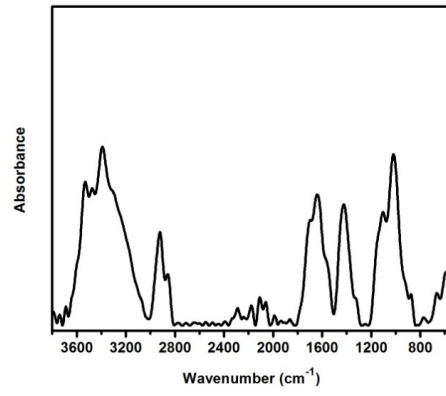
Domatius icon are shown in Fig. 4, 5 and 6 respectively. FTIR spectra of all samples indicated the presence of bands of N-H stretching in the range of 3300-3400 cm⁻¹, amide C=O stretching (amide I) in the range of 1700-1600 cm⁻¹ and amide N-H bending (amide II) in the range of 1600-1500 cm⁻¹, indicating the presence of a proteinaceous material which is corresponding to the material used as the binder, mostly egg yolk [3]. The obtained FTIR spectra of all samples also indicated the presence of metal species

reflected by the bands arising in the range of 1200-400 cm^{-1} [27] thus confirming the results obtained by EDS and XRF.

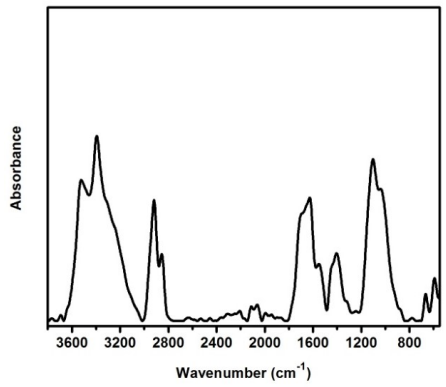
The obtained FTIR bands for samples from Saint Abaskhiroun icon, Saint George icon and Saints Maximus and Domatius icon are illustrated in Tables 8, 9 and 10 respectively.



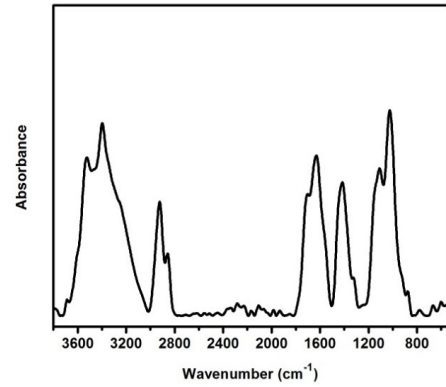
Sample 1



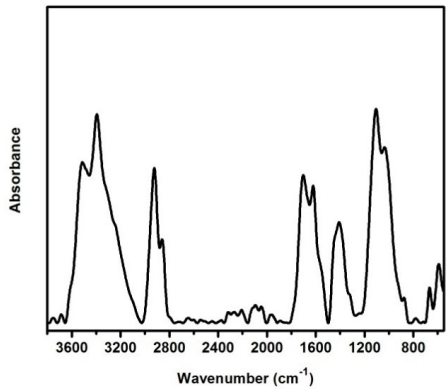
Sample 2



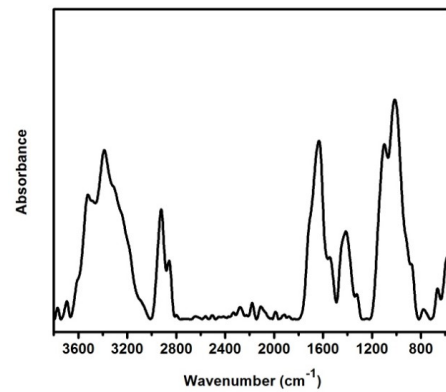
Sample 3



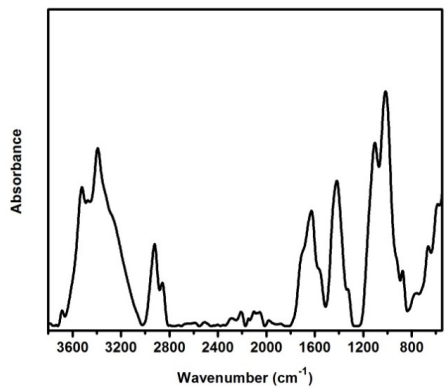
Sample 4



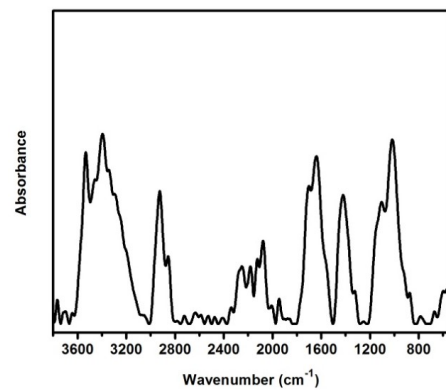
Sample 5



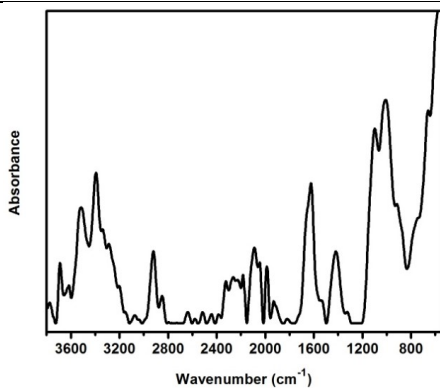
Sample 6



Sample 7



Sample 8

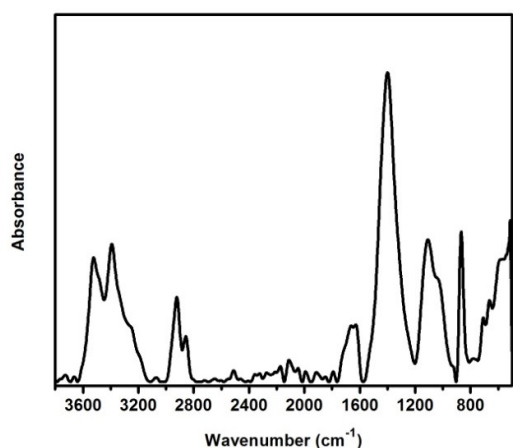


Sample 9

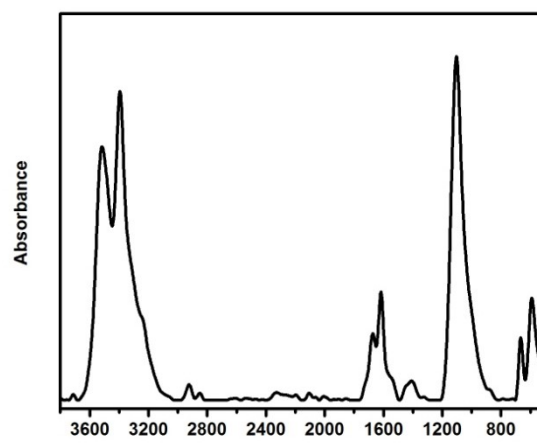
Figure 4. FTIR absorbance spectra of sample 1 to 9 from Saint Abaskhiroun icon.

Table 8. FTIR band assignment of samples 1 to 9 from Saint Abaskhiroun icon

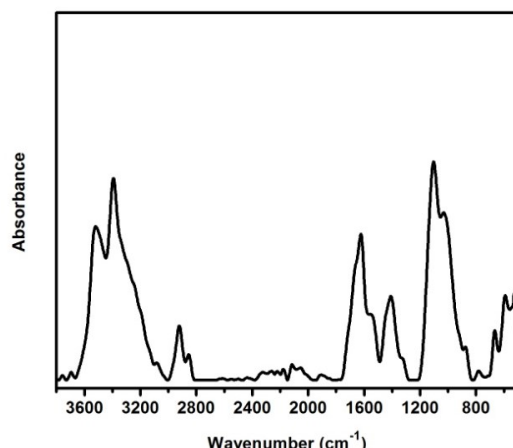
Characteristic band (cm ⁻¹)									Assignment
1	2	3	4	5	6	7	8	9	
3526	3531	3523	3525	3513	3521	3522	3531	3515	O-H stretching vibration of Water
3395	3391	3394	3397	3395	3386	3392	3394	3393	N-H stretching vibration
2926	2923	2919	2924	2924	2924	2923	2925	2921	C-H asymmetric stretching vibration
2862	2859	2855	2859	2861	2860	2860	2856	2851	C-H symmetric stretching vibration
1633	1641	1627	1631	1702	1633	1627	1639	1623	Amide I
1557	1553	1551	1559	1621	1545	1561	1557	1545	Amide II
1439	1412	1404	1417	1408	1413	1419	1419	1419	C-H bending vibration of CH ₂
1325	1315	1321	1325	1321	1325	1327	1325	1325	C-H bending vibration of CH ₃



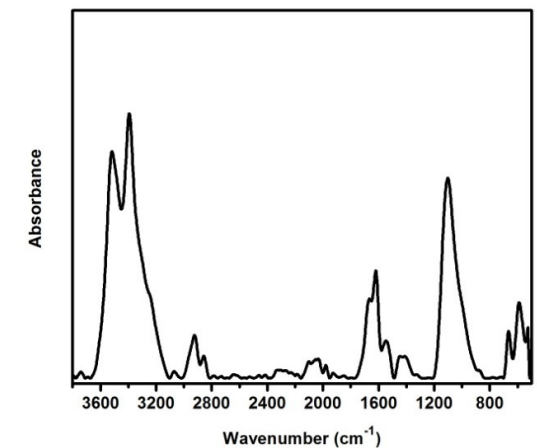
Sample 1



Sample 2



Sample 3



Sample 4

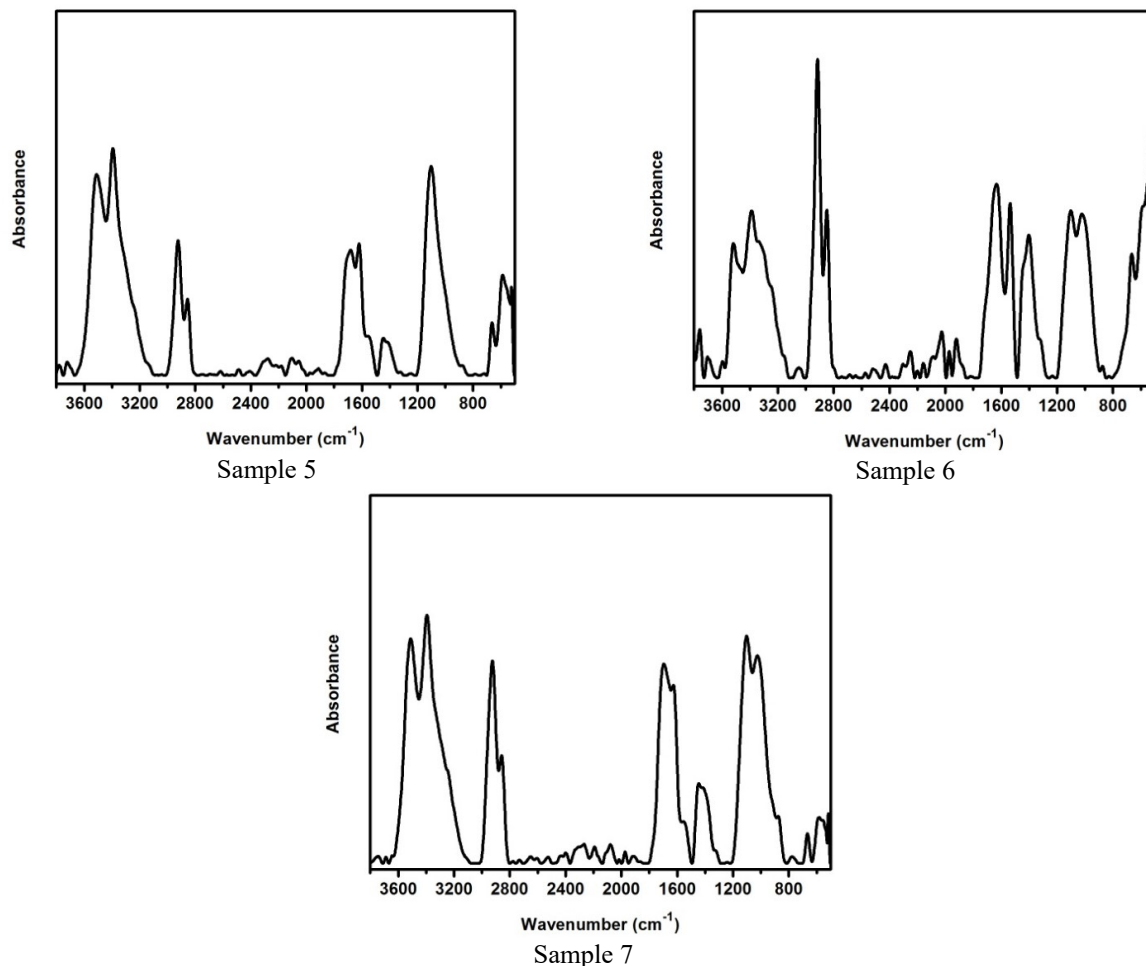
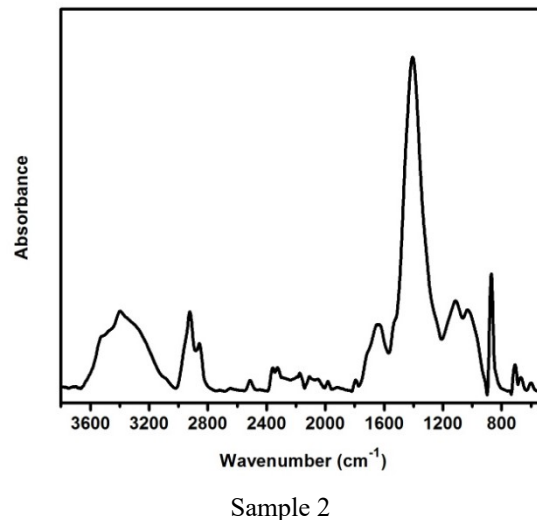
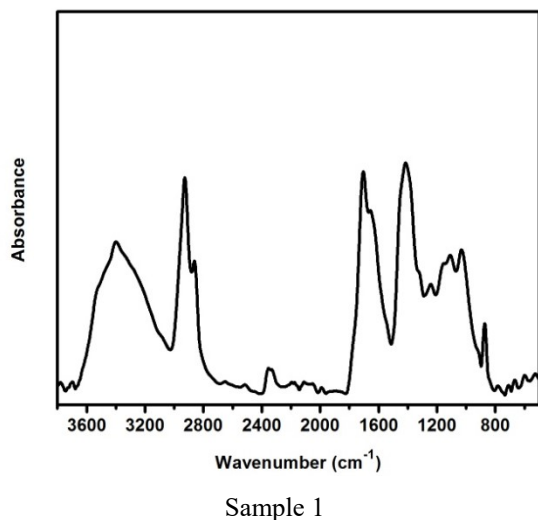
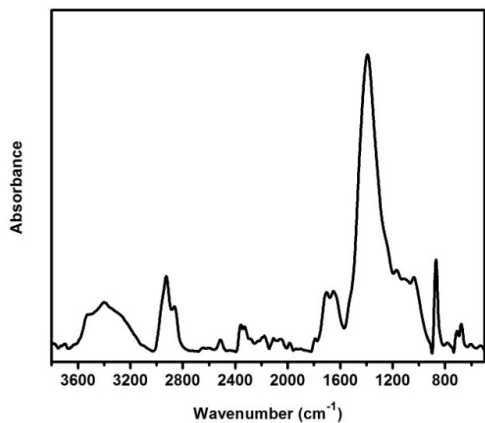


Figure 5. FTIR absorbance spectra of sample 1 to 7 from Saint George icon.

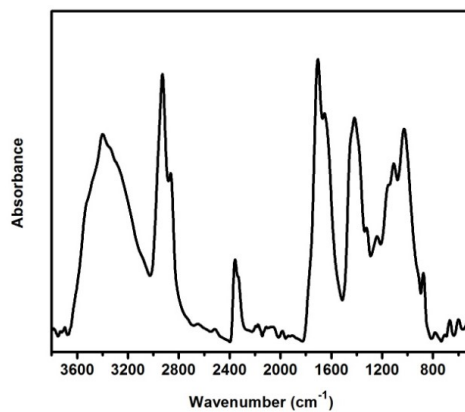
Table 9. FTIR band assignment of samples 1 to 7 from Saint George icon

Characteristic band (cm ⁻¹)							Assignment
1	2	3	4	5	6	7	
3523	3516	3518	3517	3509	3519	3511	O-H stretching vibration of Water
3390	3394	3392	3393	3393	3388	3395	N-H stretching vibration
2922	2924	2922	2923	2924	2916	2925	C-H asymmetric stretching vibration
2857	2852	2856	2857	2856	2849	2859	C-H symmetric stretching vibration
1662	1670	1623	1619	1621	1633	1627	Amide I
1629	1616	1553	1544	1556	1535	1555	Amide II
1396	1408	1407	1413	1445	1402	1445	C-H bending vibration of CH ₂
--	1325	1325	1327	1323	1317	1317	C-H bending vibration of CH ₃

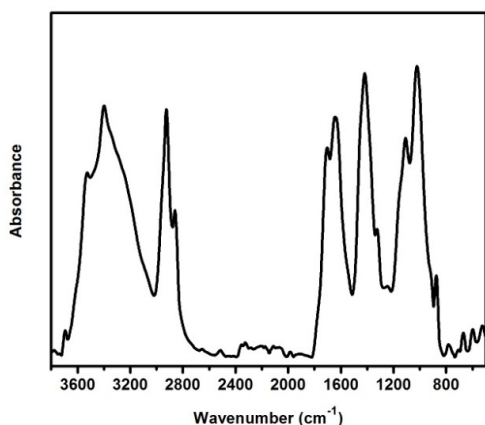




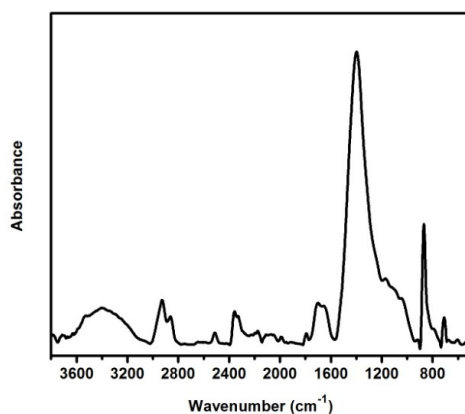
Sample 3



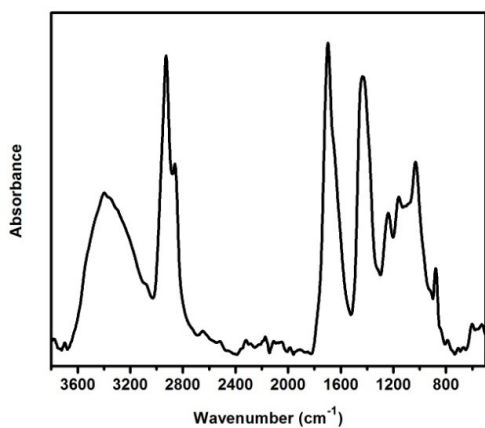
Sample 4



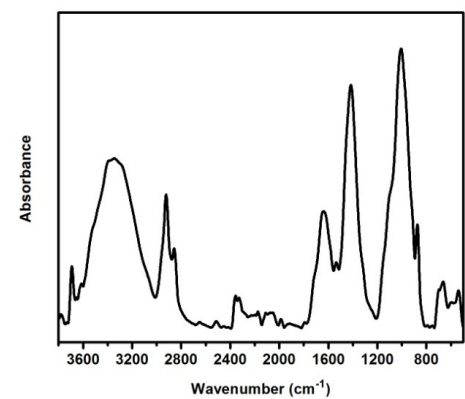
Sample 5



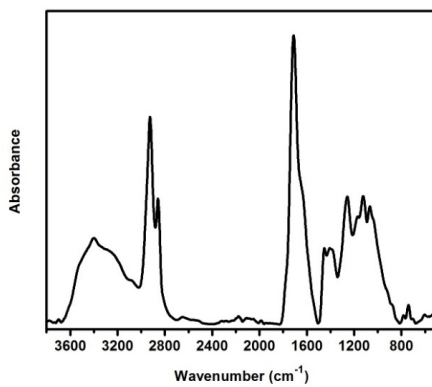
Sample 6



Sample 7



Sample 8



Sample 9

Figure 6. FTIR absorbance spectra of sample 1 to 8 from Saints Maximus and Domatius icon

Table 10. FTIR band assignment of samples 1 to 8 from Saints Maximus and Domatius icon

Characteristic band (cm ⁻¹)									Assignment
1	2	3	4	5	6	7	8	9	
	3500	3500		3500	3500		3588		O-H stretching vibration of Water
3366	3362	3366	3366	3364	3370	3362	3309	3364	N-H stretching vibration
2927	2923	2926	2928	2925	2927	2928	2923	2924	C-H asymmetric stretching vibration
2862	2858	2863	2864	2860	2862	2861	2857	2864	C-H symmetric stretching vibration
1574	1667	1572	1574	1572	1570	1565	1667	1580	Amide I
1523	1515	1517	1519	1510	1525	--	1502	--	Amide II
--	--	--	--	--	--	--	1394	--	C-H bending vibration of CH ₂
--	--	--	--	--	--	--	--	1307	C-H bending vibration of CH ₃

3.3.1. Deconvolution of FTIR spectra.

In order to further confirm the results obtained through FTIR, EDS and XRF analyses, self-deconvolution method was applied. Fourier self-deconvolution is a numerical method that is often applied in order to increase the resolution of the obtained spectra in which the intrinsic bandwidths are much greater than the instrumental resolution [28]. It was applied for two bands in each spectrum, namely the band corresponding to O-H stretching vibration (~3400-3600 cm⁻¹) and the band corresponding to amide I (~1600-1790 cm⁻¹).

The O-H stretching band was selected in order to evaluate the effect of aging manifested by the presence of free OH⁻ ions which appear at higher wavenumber than that of intermolecular and intramolecular OH groups. The excessive formation of free OH⁻ ions with aging makes them immediately available for interacting with different chemical species within the icons and in the surrounding environment [29].

The amide I band was also selected as it is conformationally sensitive, thus commonly used to characterize the variation of the secondary structure in proteins and polypeptides [30], and so in this study a special attention was given to this band in order to study the interaction occurring through it between the metal oxides, supposedly present in the paint materials, and the binder which would results in a new band at a slightly higher wavenumber than that of amide I band. The selected bands both before and after deconvolution are shown in tables 11, 12 and 13.

As seen in table 11, the O-H stretching vibration band of samples 2, 7, 8 and 9 of Saint Abaskhiroun icon did not require

undergoing deconvolution because in each sample there are already two distinct bands at 3519 cm⁻¹ and 3596 cm⁻¹ corresponding to O-H stretching vibration of water molecule and O-H stretching vibration of free OH. Similarly, the amide I vibration band of samples 1, 2, 3, 4, 5 and 8 did not also require to undergo deconvolution due to the presence of two distinct bands in this region for each of those samples.

As shown in table 12, the O-H stretching vibration band of sample 6 of Saint George icon did not require undergoing deconvolution because there are already two distinct bands in this region at 3519 cm⁻¹ and 3596 cm⁻¹ corresponding to O-H stretching vibration of water molecule and O-H stretching vibration of free OH respectively. Also, as seen in the same table, the amide I band of samples 4, 5 and 7 did not require undergoing deconvolution because the amide I band of each sample clearly consisted of bands at 1663 cm⁻¹ and 1619 cm⁻¹ for sample 4, 1682 cm⁻¹ and 1621 cm⁻¹ for sample 5, and 1696 cm⁻¹ and 1627 cm⁻¹ for sample 7.

As shown in Table 13, the O-H stretching vibration band of sample 5 of Saints Maximus and Domatius Icon did not need deconvolution as there are already two discrete bands at 3676 cm⁻¹ and 3499 cm⁻¹ corresponding to O-H stretching vibration of free OH and O-H stretching vibration of water molecule respectively. The amide I vibration band of samples 3 and sample 6 also did not need deconvolution as there are two distinct bands in this region for each sample, being at 1663 cm⁻¹ and 1572 cm⁻¹ for sample 3, and at 1667 cm⁻¹ and 1570 cm⁻¹ for sample 6.

Table 11. FTIR band positions before and after deconvolution of samples from Saint Abaskhiron Icon

Sample	Band position (cm ⁻¹)					
	O-H stretching vibration			Amide I		
	Before	After		Before	After	
Sample 1	3526	3600	3535	--	--	--
Sample 2	--	--	--	--	--	--
Sample 3	3523	3588	3533	--	--	--
Sample 4	3525	3609	3535	--	--	--
Sample 5	3513	3615	3525	--	--	--
Sample 6	3521	3613	3529	1633	1716	1623
Sample 7	--	--	--	1627	1714	1621
Sample 8	--	--	--	--	--	--
Sample 9	--	--	--	1623	1667	1619

Table 12. FTIR band positions before and after deconvolution of samples from Saint George Icon

Sample	Band position (cm ⁻¹)					
	O-H stretching vibration			Amide I		
	Before	After		Before	After	
Sample 1	3523	3605	3527	1662	1725	1672
Sample 2	3516	3596	3525	1670	1731	1676

Sample	Band position (cm ⁻¹)					
	O-H stretching vibration			Amide I		
	Before	After		Before	After	
Sample 3	3518	3598	3531	1621	1669	1619
Sample 4	3517	3598	3525	--	--	--
Sample 5	3509	3637	3521	--	--	--
Sample 6	--	--	--	1633	1657	1621
Sample 7	3511	3592	3515	--	--	--

Table 13: Saints Maximus and Domatius Icon FTIR band positions before and after deconvolution

Sample	Band position (cm ⁻¹)					
	O-H stretching vibration			Amide I		
	Before	After		Before	After	
Sample 1	3366	3507	3433	1704	1649	1578
Sample 2	3500	3505	3441	1667	1723	1668
Sample 3	3500	3566	3509	--	--	--
Sample 4	3366	3507	3437	1574	1649	1578
Sample 5	--	--	--	1572	1651	1582
Sample 6	3500	3566	3511	--	--	--
Sample 7	3362	3509	3427	1565	1651	1568
Sample 8	3588	3596	3501	1667	1667	1586
Sample 9	3364	3590	3501	1580	1655	1582

3.4. Molecular Modeling Study.

Molecular modelling simulations were used to describe the interaction between aspartic amino acid, contained in the binder, and aluminum, iron and zinc oxides, supposedly contained in the paint layer. Fig. 7 and 8 show three metal oxides, namely Fe₂O₃, Al₂O₃ and ZnO, interacting with aspartic amino acid without and with hydration, respectively.

The interaction takes place through the hydrogen bonding of COOH and NH₂. The first carboxyl group is bridging onto Al₂O₃ while the second is bridging onto Fe₂O₃. ZnO is supposed to interact with aspartic acid through one hydrogen of NH₂ group. When hydration takes place, 7 water molecules form a weak interaction as shown in Fig. 8.

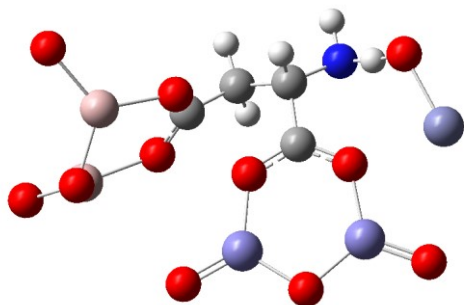


Figure 7. Results of molecular modeling simulations: iron, aluminum and zinc oxides interacting with aspartic amino acid without water molecules.

Technical details are given elsewhere [31]; here we want to remark that the structure remains reactive even after hydration with 7 water molecules and is potentially capable of causing severe deterioration of the painting layer. While the findings of [31], need more verification in case of the interaction between amino acid and more than one metal oxide as indicated in the last research. As shown in table 14, the interaction between three metal oxides and amino acid show optimized structure at B3LYP/6-31g(d,p) the total dipole moment was 13.3374 Debye while the HOMO/LUMO band gap is 0.4065 eV. As far as water

molecules interact with this configuration these values became 12.7158 Debye and 0.3967 eV respectively.

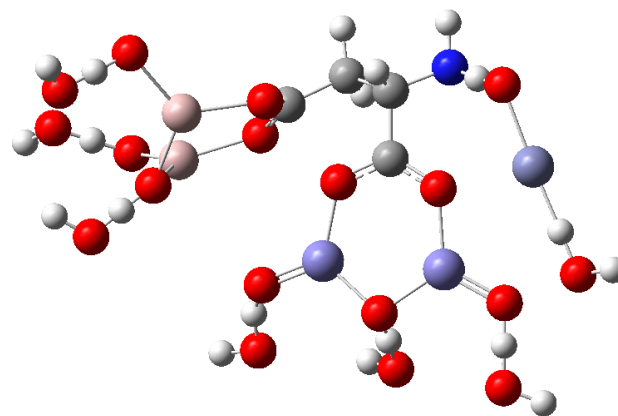


Figure 8. Results of molecular modeling simulations: iron, aluminum and zinc oxides interacting with aspartic amino acid with water molecules

The correlation between physical parameters such as total dipole moment and HOMO/LUMO band gap energies is discussed in detail earlier [32]. It is stated that higher values of total dipole moment with lower values of HMO/LUMO indicated that such molecular systems could further interact with its surrounding molecules. According to the calculations, the total dipole moment of the resulting coordination compound is high, while HOMO/LUMO band gap energy is decreased as water interacted with metal oxides/amino acid, thus increasing its reactivity to interact with the environment, in particular with water molecules from environmental humidity. This interaction may cause severe deterioration of the painting.

As indicated by the presented data, molecular modeling show the ability to confirm the experimental (FTIR, SEM-EDS, XRF) results this is not limited to cultural heritage but also for several systems whereas multidisciplinary work is needed [33-38].

Table 14. B3LYP/6-31g(d,p) total dipole moment (TDM) as Debye and Band gap energy (ΔE) as eV for the studied structure.

Studied structures	TDM	ΔE
Iron, aluminium and zinc oxides/aspartic acid	13.3374	0.4065
Iron, aluminum and zinc oxides/aspartic acid/water	12.7158	0.3967

4. CONCLUSIONS

Studying and tracking the effect of aging on Coptic icons is very crucial for conservation/restoration processes and to avoid future deterioration of the icons for the same reasons. SEM micrographs of the samples obtained the three icons demonstrated the effect of aging reflected by the presence of microcracks owing to the cement-like nature of the ground layers of the icons. EDS and XRF analyses confirmed that the ground layer of the icons is made of gypsum and lead white. The binder was found to be egg yolk which was confirmed by EDS analysis that indicated the presence of an organic component and further confirmed by FTIR which showed the characteristic bands of a protein. XRF and EDS analysis indicated the presence of several metals, mostly metal oxides, in the paint layer. FTIR confirmed the presence of metal oxides reflected by their characteristic bands in the obtained spectra. DFT molecular modeling calculations of the interaction of aluminium, iron and zinc oxides with aspartic amino acid both in adsorbed and complex states, with and without hydration indicated that the reactivity of the resultant coordinated compounds under the effect of hydration from humidity is significantly increased

due to conversion of metal oxides into metal hydroxides. Deconvolution of O-H stretching vibration band and amide I band in the FTIR spectra of most of the samples confirmed the computational resulting through indicating the presence of bands characteristic for free OH ions as well as the presence of bands characteristic for conformationally altered amide I band suggesting the interaction with the metal oxides of the paint layer. Molecular modeling was used to describe the interaction between aspartic acid which is contained in the binder of a painting layer, and aluminum, iron and zinc oxides which are contained in the pigments. Calculated total dipole moment of the resulting coordinated compound increases, accordingly the capability of interaction increased with the surrounding environment. Particular with water from environmental humidity, this interaction may cause severe deterioration of the painting. So, this proposed mechanism of the effect of hydration from humidity on the resultant coordinated compounds in the paint layer is suggested to be a major cause of the severe deterioration of the icons with time.

5. REFERENCES

- Abdel-Ghani, M.; Edwards, H.G.M.; Janaway, R.; Stern, B. A Raman microscopic and gas chromatographic–mass spectrometric study of two 19th century overlapping Coptic icons of Anastasy Al-Romi. *Vib. Spectrosc.* **2008**, *48*, 69–75, <https://doi.org/10.1016/j.vibspec.2008.02.013>.
- Sakr, A.A.; Ghaly, M.F.; Geight, E.F.; Abdel-Haliem, M.E.F. Characterization of grounds, pigments, binding media, and varnish coating of the Angel Michael' icon, 18th century, Egypt. *Journal of Archaeological Science: Reports* **2016**, *9*, 347–357, <http://dx.doi.org/10.1016/j.jasrep.2016.08.039>.
- Issa, Y.M.; Abdel-Maksoud, G.; Magdy, M. Analytical study of Saint Gregory Nazianzen Icon, Old Cairo, Egypt. *J. Mol. Struct.* **2015**, *1100*, 70-79, <http://dx.doi.org/10.1016/j.molstruc.2015.07.004>.
- Abdel-Ghani, M.; Stern, B.; Edwards, H.G.M.; Janaway, R. A study of 18th century Coptic icons of Ibrahim Al-Nasekh using Raman microscopy and gas chromatography–mass spectrometry: Indigo as an organic pigment in Egyptian panel paintings. *Vib. Spectrosc.* **2012**, *62*, 98–109, <http://dx.doi.org/10.1016/j.vibspec.2012.05.003>.
- Abdel-Ghani, M.; Edwards, H.G.M.; Stern, B.; Janaway, R. Characterization of paint and varnish on a medieval Coptic-Byzantine icon: Novel usage of dammar resin. *Spectrochim. Acta A* **2009**, *73*, 566–575, <https://doi.org/10.1016/j.saa.2008.10.050>.
- Gulzar, S.; Burg, J.P. Preliminary investigation of late Mughal period wall paintings from historic monuments of Begumpura, Lahore. *Frontiers of Architectural Research* **2018**, *7*, 465–472, <https://doi.org/10.1016/j.foar.2018.08.001>.
- Mikayama, A.; Hokoi, S.; Ogura, D.; Okada, K.; Su, B. Effects of Drifting Sand Particles on Deterioration of Mural Paintings on the East Wall of Cave 285 in Mogao Caves, Dunhuang. *Enrgy Proced.* **2015**, *78*, 1311-1316, <https://doi.org/10.1016/j.egypro.2015.11.146>.
- Sterflinger, K.; Piñar, G. Microbial deterioration of cultural heritage and works of art — tilting at windmills? *Appl. Microbiol. Biotechnol.* **2013**, *97*, 9637–9646, <https://doi.org/10.1007/s00253-013-5283-1>.
- Sterflinger, K. Fungi: Their role in deterioration of cultural heritage. *Fungal Biol. Rev.* **2010**, *24*, 47-55, <https://doi.org/10.1016/j.fbr.2010.03.003>.
- Petronela, S.; Sandu, I.; Stratulat, L. The conscious deterioration and degradation of the cultural heritage. *International Journal of Conservation Science* **2017**, *8*, 81-88.
- Bakr, A-M.; Kawiak, T.; Pawlikowski, M.; Sawlowicz, Z. Characterisation of 15th century red and black pastes used for wall decoration in the Qijmas El-Eshaqi mosque (Cairo, Egypt). *J. Cult. Herit.* **2005**, *6*, 351-356, <https://doi.org/10.1016/j.culher.2004.12.002>.
- Ahmed, H.E.; Ziddan, Y.E. A new approach for conservation treatment of a silk textile in Islamic Art Museum, Cairo. *J. Cult. Herit.* **2011**, *12*, 412-419, <https://doi.org/10.1016/j.culher.2011.02.004>.
- Abdel-Maksoud, G.; Abdel-Hady, M. Effect of burial environment on crocodile bones from Hawara excavation, Fayoum, Egypt. *J. Cult. Herit.* **2011**, *12*, 180-189, <https://doi.org/10.1016/j.culher.2010.12.002>.
- Fantacci, S.; Amat, A.; Sgamellotti, A. Computational Chemistry Meets Cultural Heritage: Challenges and Perspectives. *Acc. Chem. Res.* **2010**, *43*, 802–813, <https://doi.org/10.1021/ar100012b>.
- Hajjar, L.; Hicks, R.G.; Zeng, T. A Computational Study of the Protoisomerization of Indigo and Its Imine Derivatives. *J. Phys. Chem. A* **2016**, *120*, 7569–7576, <https://doi.org/10.1021/acs.jpca.6b07838>.
- Jurinovich, S.; Degano, I.; Mennucci, B. A Strategy for the Study of the Interactions between Metal–Dyes and Proteins with QM/MM Approaches: the Case of Iron–Gall Dye. *J. Phys. Chem. B* **2012**, *116*, 13344–13352, <https://doi.org/10.1021/jp3083002>.
- Jiwalak, N.; Daengngern, R.; Rungrotmongkol, T.; Jungstittiwong, S.; Namuangruk, S.; Kungwan, N.;

Dokmaisrijan, S. A spectroscopic study of indigo dye in aqueous solution: A combined experimental and TD-DFT study. *J. Lumin.* **2018**, *204*, 568-572, <https://doi.org/10.1016/j.jlumin.2018.08.060>.

18. Pintus, A.; Aragoni, M.C.; Carcangiu, G.; Giacobetti, L.; Isaia, F.; Lippolis, V.; Maiore, L.; Meloni, P.; Arca, M. Density functional theory modelling of protective agents for carbonate stones: a case study of oxalate and oxamate inorganic salts. *New J. Chem.* **2018**, *42*, 11593-11600, <https://doi.org/10.1039/C8NJ01714J>.

19. Galal, A.M.F.; Atta, D.; Abouelsayed, A.; Ibrahim, M.A.; Hanna, A.G. Configuration and Molecular Structure of 5-Chloro-N-(4-sulfamoylbenzyl) Salicylamide Derivatives. *Spectrochim. Acta A* **2019**, *214*, 476-486, <https://doi.org/10.1016/j.saa.2019.02.070>.

20. Abdelsalam, H.; Teleb, N.H.; Yahia, I.S.; Zahran, H.Y.; Elhaes, H.; Ibrahim, M.A. First principles study of the adsorption of hydrated heavy metals on graphene quantum dots. *J. Phys. Chem. Solids* **2019**, *130*, 32-40, <https://doi.org/10.1016/j.jpcs.2019.02.014>.

21. Abdelsalam, H.; Saroka, V.A.; Ali, M.; Teleb, N.H.; Elhaes, H.; Ibrahim, M.A. Stability and electronic properties of edge functionalized silicene quantum dots: A first principles study. *Physica E* **2019**, *108*, 339-346, <https://doi.org/10.1016/j.physe.2018.07.022>.

22. Frisch, M.; Trucks, G.; Schlegel, H.; Scuseria, G.; Robb, M.; Cheeseman, J.; Scalmani, G.; Barone, V.; Mennucci, B.; Petersson, G.; Nakatsuji, H.; Caricato, M.; Li, X.; Hratchian, H.; Izmaylov, A.; Bloino, J.; Zheng, G.; Sonnenberg, J.; Hada, M.; Ehara, M.; Toyota, K.; Fukuda, R.; Hasegawa, J.; Ishida, M.; Nakajima, T.; Honda, Y.; Kitao, O.; Nakai, H.; Vreven, T.; Montgomery Jr, J.; Peralta, J.; Ogliaro, F.; Bearpark, M.; Heyd, J.; Brothers, E.; Kudin, K.; Staroverov, V.; Keith, T.; Kobayashi, R.; Normand, J.; Raghavachari, K.; Rendell, A.; Burant, J.; Iyengar, S.; Tomasi, J.; Cossi, M.; Rega, N.; Millam, J.; Klene, M.; Knox, J.; Cross, J.; Bakken, V.; Adamo, C.; Jaramillo, J.; Gomperts, R.; Stratmann, R.; Yazyev, O.; Austin, A.; Cammi, R.; Pomelli, C.; Ochterski, J.; Martin, R.; Morokuma, K.; Zakrzewski, V.; Voth, G.; Salvador, P.; Dannenberg, J.; Dapprich, S.; Daniels, A.; Farkas, O.; Foresman, J.; Ortiz, J.; Cioslowski, J.; Fox, D. Gaussian 09 Revision C.01, Gaussian Inc. **2010**, Wallingford CT.

23. Becke, A.D. A new mixing of Hartree-Fock and local density functional theories. *J. Chem. Phys.* **1993**, *98*, 1372-1377, <https://doi.org/10.1063/1.464304>.

24. Lee, C.; Yang, W.; Parr, R.G. Development of the Colle-Salvetti correlation-energy formula into a functional of the electron density. *Phys. Rev. B* **1988**, *37*, 785-789, <https://doi.org/10.1103/PhysRevB.37.785>.

25. Miehlich, B.; Savin, A.; Stoll, H.; Preuss, H. Results obtained with the correlation energy density functionals of Becke and Lee, Yang and Parr. *Chem. Phys. Lett.* **1989**, *157*, 200-206, [https://doi.org/10.1016/0009-2614\(89\)87234-3](https://doi.org/10.1016/0009-2614(89)87234-3).

26. Ferretti, M.; The investigation of ancient metal artefacts by portable X-ray fluorescence devices. *J. Anal. At.*

Spectrom. **2014**, *29*, 1753-1766. <https://doi.org/10.1039/c4ja00107a>.

27. Gendreau, R.M.; Jakobsen, R.J.; Henry, W.M.; Knapp, K.T. Fourier transform infrared spectroscopy for inorganic compound speciation. *Environ. Sci. Technol.* **1980**, *14*, 990-995, <https://doi.org/10.1021/es60168a008>.

28. Friesen, W.I.; Michaelian, K.H. Fourier deconvolution of photoacoustic FTIR spectra. *Infrared Phys.* **1986**, *26*, 235-242, [https://doi.org/10.1016/0020-0891\(86\)90075-8](https://doi.org/10.1016/0020-0891(86)90075-8).

29. Baglioni, P.; Chelazzi, D.; Giorgi, R. *Nanotechnologies in the Conservation of Cultural Heritage: A compendium of materials and techniques*. Springer, Netherlands, 2014.

30. Wu, Y.; Xu, Y.; Wang, D.; Zhao, Y.; Weng, S.; Xu, D.; Wu, J. FT-IR spectroscopic investigation on the interaction between nylon 66 and lithium salts. *J. Appl. Polym. Sci.* **2004**, *91*, 2869-2875, <https://doi.org/10.1002/app.13495>.

31. Mahmoud, A.A.; Osman, O.; Elhaes, H.; Ferretti, M.; Fakhry, A.; Ibrahim, M.A. Computational Analyses for the Interaction Between Aspartic Acid and Iron. *J. Comput. Theor. Nanosci.* **2018**, *15*, 470-473, <https://doi.org/10.1166/jctn.2018.7113>.

32. Ibrahim, M.A.; Mahmoud, A-A. Computational Notes on the Reactivity of some Functional Groups. *J. Comput. Theor. Nanosci.* **2009**, *6*, 1523-1526, <https://doi.org/10.1166/jctn.2009.1205>.

33. Badry, R.; El-Khodary, S.; Elhaes, H.; Nada, N.; Ibrahim, M. The Influence of Moisture on the Electronic Properties of Monomer, Dimer, Trimer and Emeraldine Base Sodium Carboxymethyl Cellulose. *Egyptian Journal of Chemistry* **2019**, *62*, 39-56, <https://doi.org/10.33263/LIANBS8.553557>.

34. Grenni, P.; Caracciolo, A.B.; Mariani, L.; Cardoni, M.; Ricucci, C.; Elhaes, H.; Ibrahim, M.A. Effectiveness of a new green technology for metal removal from contaminated water. *Microchemical Journal* **2019**, *147*, 1010-1020, <https://doi.org/10.1016/j.microc.2019.04.026>.

35. Afzal, M.A.F.; Hachmann, J. Benchmarking DFT approaches for the calculation of polarizability inputs for refractive index predictions in organic polymers. *Phys. Chem. Chem. Phys.* **2019**, *21*, 4452-4460, <https://doi.org/10.1039/C8CP05492D>.

36. Fahim, A.M.; Shalaby M.A.; Ibrahim, M. Microwave-assisted synthesis of novel 5-aminouracil-based compound with DFT calculations. *J. Mol. Struct.* **2019**, *1194*, 211-226, <https://doi.org/10.1016/j.molstruc.2019.04.078>.

37. Ari, H.; Büyükmumcu, Z. Comparison of DFT functionals for prediction of band gap of conjugated polymers and effect of HF exchange term percentage and basis set on the performance. *Computational Materials Science* **2017**, *138*, 70-76, <https://doi.org/10.1016/j.commatsci.2017.06.012>.

38. Youness, R.A.; Taha, M.A.; Ibrahim, M. In vitro bioactivity, molecular structure and mechanical properties of zirconia-carbonated hydroxyapatite nanobiocomposites sintered at different temperatures, *Materials Chemistry and Physics*, **2020**, *239*, 122011. <https://doi.org/10.1016/j.matchemphys.2019.122011>

6. ACKNOWLEDGEMENTS

This work is funded in the frameworks of: a) the Academy of Scientific Research and Technology, Egypt, ASRT Initiative, grant number 1394 and b) the CNR-NRC 2016-2017 Bilateral Project "Joint instrumental investigation of museum collections as a means of enhancing Cultural Heritage and strengthening interdisciplinary collaboration".



© 2019 by the authors. This article is an open access article distributed under the terms and conditions of the Creative Commons Attribution (CC BY) license (<http://creativecommons.org/licenses/by/4.0/>).